Millimeter-Wave Network Analysis using Nonlinear Transmission Lines

M.J.W. Rodwell, R. Yu, M. Reddy, J. Pusl[1], S. Allen, M. Case[2], U. Bhattacharya

Department of Electrical and Computer Engineering,
University of California, Santa Barbara, CA 93106

ABSTRACT

We report systems for network measurements at millimeter-wave frequencies. Active probes are used for on-wafer measurements to approximately 150 GHz. The active probes incorporate monolithic GaAs mm-wave network analysis circuits (comprising a nonlinear transmission line stimulus signal generator and a directional sampling circuit) and low-loss, rugged quartz coplanar-waveguide probe tips. Wideband transmitter and receiver integrated circuits, incorporating nonlinear transmission lines and sampling circuits interfaced to frequency-independent antennas, are used for free-space transmission measurements to approximately 250 GHz.

I. INTRODUCTION

Power-gain cutoff frequencies of heterostructure transistors have exceeded 350 GHz [1], enabling the demonstration of monolithic amplifiers and other receiver components at frequencies as high as 120 GHz. For circuit development at higher frequencies, serving applications in fiber and wireless communications, radar, and imaging, improvements in transistor bandwidth must be accompanied by development of the wideband instrumentation used for device modeling and for circuit evaluation. Monolithic millimeter-wave integrated circuits (MIMICs), in particular, demand accurate transistor and passive element models during the design phase, models which cannot be extrapolated with great confidence from measurements at lower frequencies.

Limited instrumentation is a particularly pressing difficulty in the design of the sub-mm-wave mixers and frequency multipliers used for radio astronomy and atmospheric remote sensing. Device RF models are frequency extrapolated from DC measurements and circuit impedances usually cannot be measured, thus mixers and multipliers are empirically adjusted using waveguide mounts with tuning screws.

Sampling oscilloscopes, network analyzers, counters, and synthesizers use diode sampling bridges for signal measurement or frequency downconversion. Instrument bandwidth is limited by sampling circuit bandwidth, in turn limited by the duration of the

---

[1]Now with Hughes Aircraft Company, Space and Communications Group, S12/W305, P.O. box 92919, Los Angeles, CA 90009.

[2]Now with Hughes Research Laboratories, 3011 Malibu Canyon Road, Malibu, CA 90265

0-7803-0894-8/93 $3.00 © 1993 IEEE

strobe pulse used to switch the diodes. Since 1966, 20-30 ps silicon step-recovery diodes (SRDs) have been used for strobe pulse generation, limiting sampling circuit bandwidth to ≈20–40 GHz.

We have developed nonlinear transmission line (NLTL) pulse generators with over a factor of 10 shorter transition times than such SRDs. The pulse trains generated by NLTLs have significant spectral content to sub-mm-wave frequencies. Using NLTLs as strobe pulse generators, sampling circuits with millimeter-wave bandwidths have been realized. NLTLs and sampling circuits are then used as signal sources and detectors for in systems for on-wafer and free-space mm-wave network analysis.

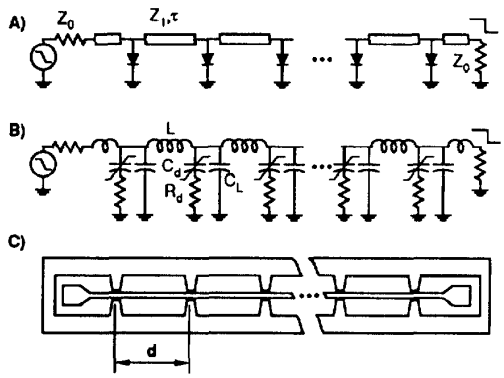

Figure 1: NLTL circuit diagram, a), equivalent circuit, b), and layout, c). C_D is the diode capacitance and R_D its series resistance, $C_L = \tau/Z_1$ is the line capacitance and $L = Z_1\tau$ the line inductance.

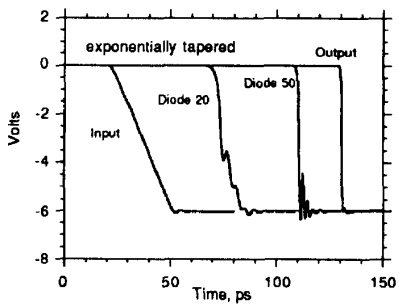

Figure 2: SPICE simulation of NLTL wavefront compression and shock-wave formation.

II. THE SHOCK-WAVE NLTL

The NLTL [2] (fig. 1) is a high-impedance transmission line periodically loaded by reverse-biased Schottky diodes acting as voltage-variable capacitors. The wave propagation velocity varies as the inverse square root of the total (diode plus transmission line) capacitance per unit length and hence increases as the diode reverse bias voltage is increased.

Given a negative-going step function (wavefront) input, the initial portions of the wavefront, near zero volts, will propagate more slowly than the final, more negative, portions of the wavefront. The wavefront transition time (falltime) will progressively decrease with propagation distance. An asymptotic (minimum) compressed falltime is eventually reached (fig. 2) at which the NLTL compression is balanced by various bandwidth limits in the structure. The two dominant bandwidth limits are the varactor diode cutoff frequency $f_D = 1/2\pi R_D C_D$ (defined using the average diode capacitance $\Delta Q/\Delta V$) and the periodic-line (Bragg) cutoff frequency $f_{per} = 1/\pi\sqrt{L(C_D + C_L)}$. If the diode cutoff frequency is dominant, the diode doping is uniform, and the wavefront is 6

Volt amplitude, the minimum compressed falltime is $T_{f,min} = 1.4/f_D$. Advanced Schottky varactor diodes attain 2-10 THz cutoff frequencies; with further work, NLTL transition times may ultimately reach 0.2–0.3 ps (1–1.5 THz signal bandwidth).

Diode design for the NLTL is a compromise between the objectives of high compression rate (small die area, low attenuation), high diode cutoff frequency (short falltimes), and reverse breakdown voltage. As the diode dimensions are reduced and the active-layer doping increased, the cutoff frequency increases but the reverse breakdown decreases. The larger capacitance variation of hyperabrupt varactors increases the NLTL compression rate (decreasing the required line length and hence both the skin loss and the die area), but hyperabrupt doping decreases the cutoff frequency and the reverse breakdown. The required diode reverse breakdown voltage is determined by the minimum strobe NLTL output voltage required to drive a 2-diode sampling bridge (≈3-4 V) and by the skin-effect losses on the NLTL. As input voltages on current NLTLs are approximately 2:1 larger than the compressed output wavefronts, approximately 8 V reverse breakdown. is required.

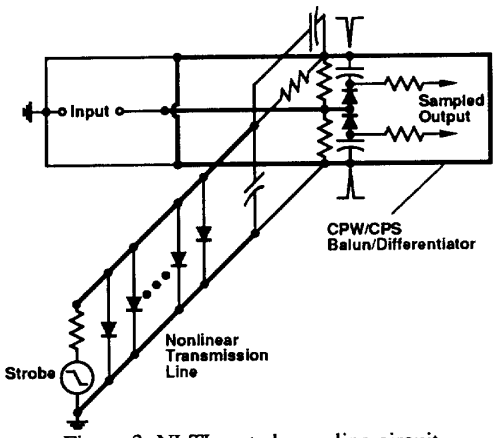

Figure 3: NLTL-gated sampling circuit

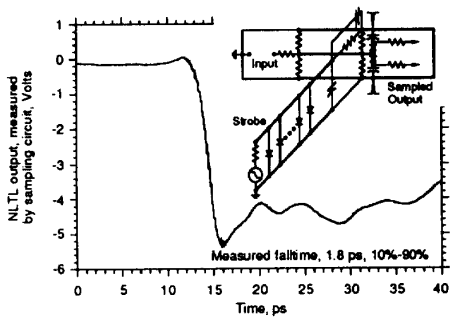

Figure 4: NLTL output measured by an NLTL-gated sampling circuit, both using hyperabrupt diode technology. The measured falltime is 1.8 ps.

III. NLTL-GATED SAMPLING CIRCUITS

A sampling circuit (fig. 3) [2] consists of a strobe pulse generator, a diode/resistor bridge, and a balun/differentiator. An NLTL compresses an input strobe signal, either a step function or a ~10 GHz sinewave, to picosecond falltimes. The sampling diodes are gated by a pair of symmetric positive and negative impulses generated from the strobe NLTL output using a balun / differentiator implemented using the coplanar strip (CPS) mode of the input signal coplanar waveguide (CPW). Coupled through series hold capacitors, the complementary strobe pulses drive the sampling diodes into forward conduction. During this period, the aperture time, the input (RF) signal partially charges the hold capacitors. If the RF frequency is then offset by Δf from a multiple nf_o of the

strobe frequency f_0, the sampled (IF) signal is mapped out at a repetition frequency Δf. Sampling circuit bandwidth is limited by the sampling diode capacitance and by the aperture time.

To evaluate the NLTL and sampling circuit risetime, the output of an NLTL shock generator is connected to an on-wafer NLTL-gated sampling circuit. The convolved responses of sampling circuit and NLTL shock-wave generator is thus measured. With an NLTL using 1.7 THz exponential hyperabrupt diodes (fig. 4), a 1.8 ps falltime is measured. From this, a 1.3 ps deconvolved NLTL falltime and a 275 GHz sampling circuit bandwidth are determined; NLTLs and sampling circuits with approximately twice this bandwidth will be reported elsewhere [3] by Allen et. al.

III. NLTL SOLITON IMPULSE COMPRESSORS

Although not employed in the current NLTL-based instruments reported here, variants of the NLTL employing soliton propagation effects are more efficient than shock-wave devices in the generation of harmonics of an input signal. Among other applications, these devices can be used as the stimulus signal for network analysis, in place of the shock-wave NLTLs used in the current work.

A solitary wave is a traveling wave having a localized transition (e.g. a pulse) and propagating without distortion in a nonlinear, dispersive medium. Solitons are defined as those solitary waves which preserve their shape and velocity after interactions with other solitons [4]. The soliton is a pulse waveform for which the effects of nonlinearity and dispersion are balanced. If the NLTL Bragg frequency is much smaller than the diode cutoff frequency then propagation is dominated by the interaction between the capacitive nonlinearity and the periodic-network dispersion, and solitons propagate [5]. On NLTLs, soliton duration is inversely proportional to the Bragg frequency and varies approximately as the inverse square root of the peak amplitude. Soliton propagation velocity increases with increasing soliton amplitude. Applied to the NLTL, signals with pulse duration longer than the duration of a soliton correspond to a nonlinear superposition of a set of solitons having differing amplitudes and velocities, and will decompose into this set of two or more solitons during propagation. Figure 5 shows a circuit simulation of a 6 V, 63 ps impulse splitting during propagation into a pair of solitons. Note that the leading output soliton has larger amplitude and shorter duration than the input signal.

A long-duration impulse input to an NLTL will decompose into its characteristic set of solitons. Longer input pulses decompose into progressively larger numbers of solitons, and impulse compression ratios are limited to approximately 2:1 on a homogeneous line. Higher compression ratios can be obtained by using step-tapered lines, consisting of a line with Bragg frequency f_{per1} cascaded with a line with Bragg frequency $f_{per2}=2f_{per1}$. The first line section performs a 2:1 pulse compression, with the second line section performing a further 2:1 compression. While higher compression ratios can be obtained by repeating this scheme in a three-step or four-step fashion, it is

more convenient to approximate such a step-tapered line by tapering the Bragg frequency continuously [6]. Figure 6 shows the output of an exponentially-tapered soliton impulse compressor.

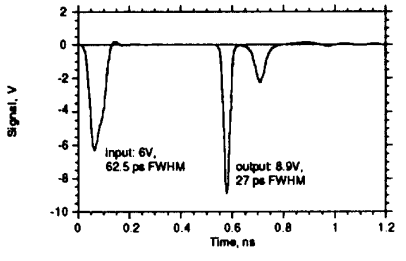

Figure 5: SPICE simulation: splitting of an input impulse into a pair of solitons during propagation on an NLTL.

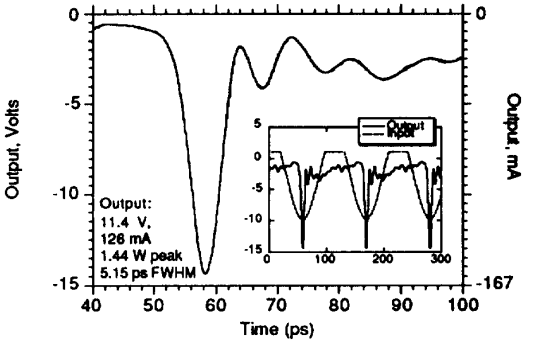

Figure 6: Measured output waveform and calculated input waveform for a tapered soliton impulse compressor

Experimental soliton NLTL output pulse durations are ≈5:1 longer than shock-wave devices, although circuit simulations predict attainable soliton durations only a factor of 1.5:1 larger than shock-wave NLTL falltimes using similar diodes. The discrepancy is not understood, although there is evidence that layout parasitics reduce Bragg frequencies by ≈2:1. If this discrepancy can be solved, soliton compressors will be much more effective than shock-wave NLTLs for high-order mm-wave frequency multiplication, as the conversion loss to the N^{th} harmonic is bounded above by 1/N for the soliton compressor, compared to $1/N^3$ for the shock-wave device.

IV. ON-WAFER MM-WAVE NETWORK ANALYSIS

Using shock-wave NLTLs and NLTL-gated sampling circuits mounted in active wafer probes, on-wafer network analysis can be performed at millimeter-wave frequencies. Figure 7 shows a typical network analyzer. A swept-frequency stimulus signal generator drives the device under test. The incident and reflected waves are separated by a directional coupler, downconverted from microwave to radio frequency by sampling circuits, and subsequently measured by RF vector voltmeters. Bandwidth limits include the sampling circuits and the frequency range of the stimulus signal generator. Available coaxial connectors also limit bandwidth; 110 GHz coaxial connectors were introduced in March 1993, with earlier connectors limited to 65 GHz.

We have developed active probes [7,8] (fig. 8) for on-wafer mm-wave vector network analysis (VNA). These contain an NLTL-based network analyzer IC and a

rugged, wideband quartz probe tip. The IC itself incorporates an NLTL stimulus signal generator and an NLTL-strobe directional sampling circuit which independently measures the forward and reverse waves from the device under test.

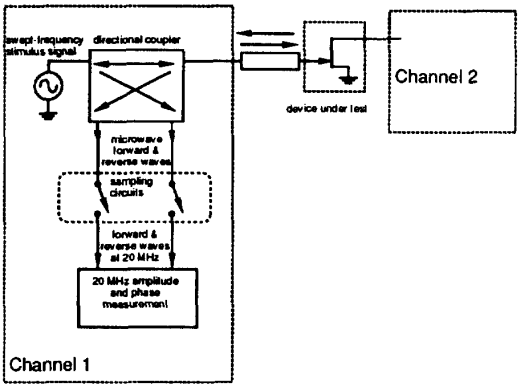

Figure 7: Simplified block diagram of a typical microwave network analyzer. Bandwidth limits are set by the signal source frequency range, by the sampling circuits, and by the coaxial connectors.

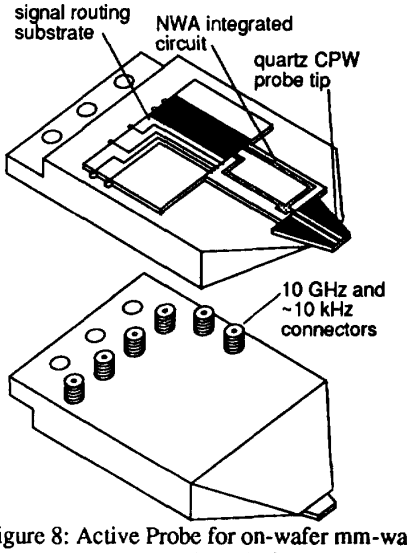

Figure 8: Active Probe for on-wafer mm-wave network analysis

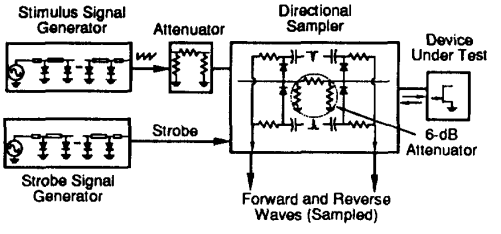

Figure 9: Block Diagram of the network analysis integrated circuit

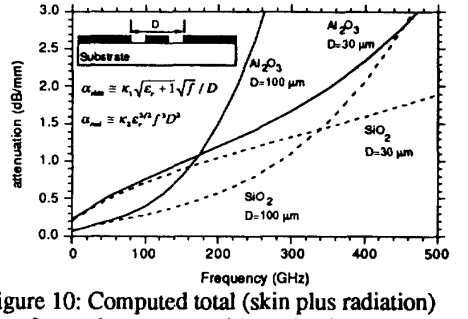

Figure 10: Computed total (skin plus radiation) losses for coplanar waveguide probe tips on quartz and alumina

The network analyzer IC block diagram is shown in figure 9. An NLTL stimulus signal generator converts a 7-14 GHz sinusoidal drive signal into a 5 V sawtooth waveform with ~2 ps transition times and with significant harmonic content to ~250 GHz. The drive signal is attenuated to levels suitable for linear characterization of transistor circuits, and is passed through a directional sampling circuit to the device under test.

The directional sampling circuit is a pair of sampling circuits measuring the port voltages of a 6 dB attenuator placed between the stimulus signal generator and the device under test. A second NLTL on the IC provides the strobe signal for the directional sampler. The attenuator port voltages $V_{out} = V_{incident} + V_{reflected}$ and $V_{in} = 2V_{incident} + V_{reflected}/2$, linear functions of the incident and reflected voltages, are downconverted by the sampling circuits to a 1 kHz intermediate frequency. The IF signals are passed through summing networks to recover $V_{incident}$ and $V_{reflected}$, and are then measured. We emphasize that the directional sampler does not obtain independent measurements of the forward and reverse waves through time-separation of pulsed signals, as in a time-domain reflectometer. Errors associated with time-gating (uncorrected terms in source and load reflections, time truncation of the long-duration impulse responses of narrowband resonators) are therefore avoided.

Tips for the active probe are coplanar waveguide (CPW) on quartz substrates. To leading order, for a given line impedance, skin loss (in dB/mm) varies as $\approx \sqrt{\varepsilon_r + 1}\sqrt{f}/D$ while radiation loss varies as $\approx \varepsilon_r^{3/2} f^3 D^2$ (fig. 10) [9], where ε_r is the relative dielectric constant of the substrate, f is frequency, and D is the ground-ground spacing of the CPW. With appropriate scaling of line dimensions, CPW on a quartz substrate (ε_r=3.8) has lower attenuation than the CPW lines on alumina substrates (ε_r=9.8) used in commercial microwave probes. At 200 GHz, D=100 μm results in a minimum 0.6 dB/mm attenuation on quartz. The probe tips have plated nickel contact bumps, plated gold airbridge ground straps for slot-line mode suppression, and the tips are angle-lapped. The 60 pH wire-bond inductance between the probe tip and the network analyzer IC is acceptable for 200 GHz measurements. Because the short quartz tips are rigid, the probes are mounted on their arms using a complaint joint.

For mm-wave measurements, the active probe stimulus NLTLs are driven at 7-14 GHz, with the strobe NLTL drive frequency offset by 1 kHz to produce an IF at this frequency. To measure device S-parameters at harmonics of the NLTL drive frequency, harmonics of the IF signals are measured by four vector voltmeters (lock-in amplifiers). The system is controlled by a desktop computer which also performs line-reflect-match calibration routines.

Figures 11-14 demonstrate system accuracy and repeatability after calibration over the 10-160 GHz range. Transmission measurements can presently be made to 160 GHz, but poor directivity prohibits measurements of return losses smaller than -20 dB at frequencies below 120 GHz. System performance is currently limited by several factors. Because of a design error, the airbridges used for probe tip slot-line mode suppression are capacitively loading the line, reducing the line impedance to 25Ω and introducing a 160 GHz cutoff; the reflection from the 25Ω loaded tip impedance seriously degrades the uncalibrated directivity. Synthesizer phase noise is also severe, corresponding to a small 1° phase deviation at 10 GHz but a large 20° deviation at 200 GHz. These factors are now being addressed.

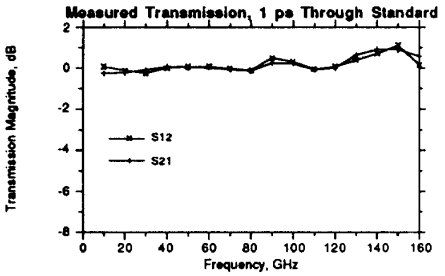

Figure 11: Measured transmission of a 1 ps through line. The deviation from 0 dB shows system accuracy.

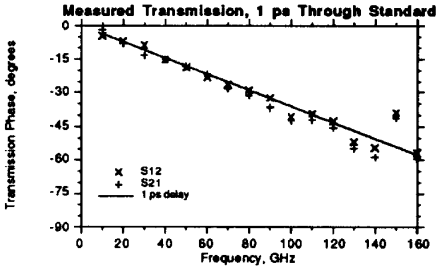

Figure 12: Measured transmission phase of the 1 ps through line. The deviation from 1 ps delay shows system accuracy.

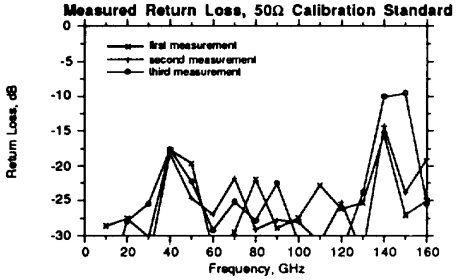

Figure 13: Measured return loss of a 50Ω calibration standard. The deviation from zero reflection (-∞ dB) shows system directivity

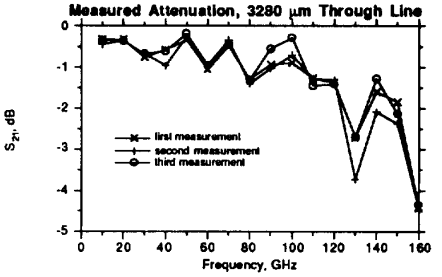

Figure 14: Measured transmission of a long coplanar line. The deviation between measurements shows system repeatability.

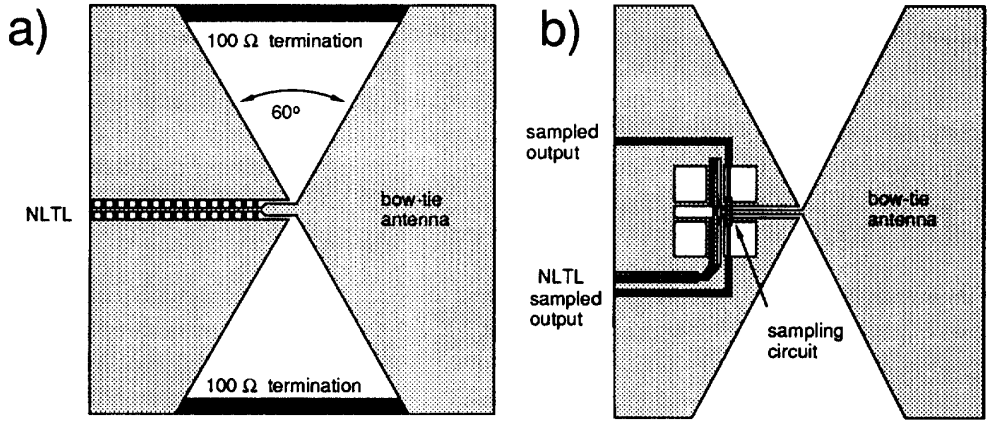

Figure 15: Simplified integrated circuit layouts of a) picosecond transmitter and b) picosecond receiver for free-space mm-wave network analysis

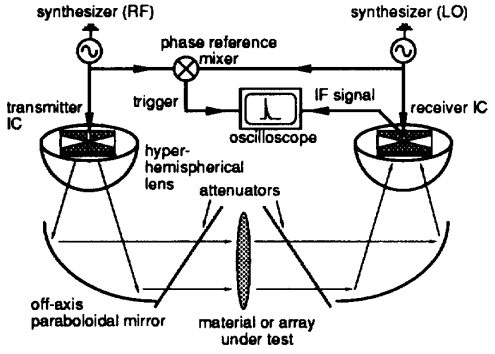

Figure 16: NLTL-based free-space network analyzer

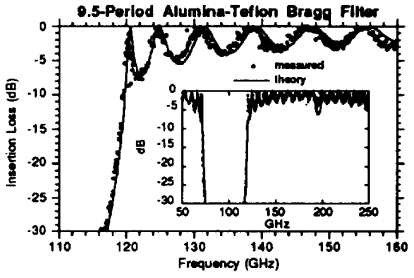

Figure 17: Transmission of a mm-wave Bragg filter

V. FREE-SPACE mm-WAVE NETWORK ANALYSIS

We have also constructed a system for gain-frequency measurements in free-space, for characterization of materials and radiating structures [10]. The system generates and detects picosecond pulses and obtains frequency information through Fourier transformation. Compared to measurement systems using mm-wave harmonic multipliers and harmonic mixers, the system is simple, relatively inexpensive, and covers a 30-250 GHz bandwidth with a single set of components.

For broadband transmission measurements in free space, the NLTL and sampling circuits must be interfaced to broadband antennas. Scale invariant antennas, including the bow-tie antenna, have frequency-independent far-field radiation patterns, and antenna impedance. The transmitter NLTL, fabricated within one electrode plane, drives the 50Ω impedance antenna, through a coplanar waveguide (CPW) balun (fig. 15,a). The receiver is a bow-tie antenna interfaced to an sampling circuit using a similar antenna feed (fig. 15,b). The system is shown in figure 16. Hyperhemispherical substrate lenses partially collimate the antenna radiation, and the radiated beam is collimated with off-axis parabolic mirrors. The receiver uses similar optics. To obtain accurate measurements, cavity resonances between the transmitter and receiver are suppressed by placing 5 dB attenuators at oblique incidence on both sides of the sample under test.

The transmitter NLTL is driven between 7 and 14 GHz, while the sampling circuit is driven at a frequency 100 Hz below the transmitter frequency. The resulting sampled 100 Hz signal is observed directly on an oscilloscope. The received signal at the sampling circuit output is a pulse train with 2.4 ps risetime. Transmission (amplitude and phase) measurements are obtained by taking the ratio of the received Fourier spectrum with the device under test in place with the spectrum of a reference measurement taken with the device under test removed. Fig. 17 shows a measurement of a high-Q Bragg filter.

VI. CONCLUSIONS

Nonlinear transmission lines and NLTL-strobed monolithic sampling circuits are *monolithic solid-state* devices for generation and measurement of electrical signals in the picosecond and millimeter-wave regimes. NLTL technology continues to improve, and 0.3 ps NLTL transition times and 1 THz sampling circuit bandwidths appear to be feasible. Based upon these, systems for sub-mm-wave on-wafer and free-space network measurements will evolve. Robust network instrumentation for device characterization and modeling is imperative for millimeter-wave and sub-mm-wave monolithic circuit design.

ACKNOWLEDGMENTS

The work was supported by the U.S. Air Force Office of Scientific Research (program number F49620-92-0464) and an associated AASERT contract, by a National Science Foundation Presidential Young Investigator Award, and by the DARPA Optoelectronics Technology Center. We acknowledge generous support from Hughes Aircraft Corporation, Wiltron, Shimadzu, Tektronix, and Hewlett-Packard Corporation.

REFERENCES

[1] U. K. Mishra, A.S. Brown, and S.E. Rosenbaum, 1988 International Electron Device Meeting, Dec. 11-14, San Francisco.
[2] Mark Rodwell, Masayuki Kamegawa, Ruai Yu, Michael Case, Eric Carman, and Kirk Giboney, IEEE Transactions on Microwave Theory and Techniques, Vol. 39, No. 7, July 1991, pp. 1194-1204.
[3] S. Allen, M. Reddy, M.J.W. Rodwell. To be presented, 1993 GaAs IC symposium, October, San Jose, CA.
[4] A.C.Scott, F.Y.F. Chu, and D.W.McLaughlin, IEEE Proc, Vol. 61, No. 10, Oct. 1973, pp. 1443-1482.
[5] R. Hirota and K. Suzuki, IEEE Proc., Vol. 61, No. 10, Oct. 1973, pp. 1483-1491.
[6] Michael Case, Eric Carman, Ruai Yu, and M.J.W. Rodwell, Applied Physics Letters, Vol. 60, no. 24, 15 June 1992, pp. 3019-3021.
[7] R.A. Marsland, C.J.Madden, D.W. Van Der Weide, M.S. Shakouri, and D. M. Bloom, 1990 GaAs IC Symposium, New Orleans, Oct. 7-10, pp. 19-22.
[8] Ruai Y. Yu, Joe Pusl, Yoshiyuki Konishi, Michael Case, Masayuki Kamegawa, and Mark Rodwell, IEEE Microwave and Guided Wave Letters, Vol. 2, No. 8, August 1992, pp. 319-321.
[9] D. B. Rutledge, D. P. Neikirk, and D. P. Kasilingam. "Integrated- Circuit Antennas" in Infrared and Millimeter Waves, K. J. Button, Ed., Vol. 10, pp. 1-90, New York: Academic Press, 1984.
[10] Y. Konishi, M. Kamegawa, M. Case, R. Yu, M.J.W. Rodwell, and D.B. Rutledge, Applied Physics Letters, Vol. 61, No 23, 7 Dec. 1992.